AVIRIS ARTIFACTS APPEARING IN LOW-LIGHT IMAGERY

Marcos J. Montes[1]

1. Introduction

AVIRIS is an excellent instrument for hyperspectral remote sensing. Its high levels of spectral resolution and energy resolution allow the detection of otherwise undetectable natural features. The high quality of the data also allows us to find artifacts in the image due to imperfections in the optics or the electronics. Researchers who work in low light (perhaps a better phrase is "low surface reflectance") environments have an opportunity to find these artifacts because the process of atmospheric correction removes most – or all – of the signal. This document lists artifacts that I have noticed when processing AVIRIS data, measured mostly over the oceans or coastal areas. When possible, I list the years the artifacts are present, and their causes. Some of the items listed below are available in previously published proceedings and they are included here because of their effects on low-light imagery.

This paper should not be interpreted in any way as saying that researchers should not use AVIRIS data. Indeed, AVIRIS is the best hyperspectral sensor for many applications. Depending on what kind of data you have, and what you do with the data, these artifacts may indeed have absolutely no effect; on the other hand, they may have a large effect on other data sets or with certain processing methods.

AVIRIS spectral and radiance calibration data is presented by the AVIRIS team both at the AVIRIS meetings, and in the various proceedings of those meetings. Note that most of the field calibration events use high-reflectance targets: several playas in California and Argentina were used for this purpose. The series of papers documenting in-flight calibration experiments includes (but is not limited to) Green and Pavri (2003, 2002, 2001, 2000), Green et al. (1999, 1998a, 1996, 1995, 1993, 1992, 1990) and Conel (1988).

Other sensors also have known artifacts, and many of these artifacts are easily visible in their published imagery. Some artifacts are corrected in post-processing, and may not appear in published imagery. Typical artifacts present in imagery from the Portable Hyperspectral Imager for Low-Light Spectroscopy (PHILLS) sensor (and how they are dealt with) are presented in Leathers et al. (2002) and Snyder et al. (2004). Many of the artifacts affecting Hyperion data are presented in several papers in the TGARS *Special Issue on the Earth Observing (EO-1) Mission* (TGARS 2003; Pearlman et al. 2003; Bindschadler et al. 2003; Green et al. 2003; Goetz et al. 2003; Datt et al. 2003; Goodenough et al. 2003). In many ways, most of the AVIRIS artifacts listed below are subtle and not obvious to the eye.

In the following sections, I will frequently mention the effect of the artifacts on atmospheric correction as applied to water (oceanic) scenes. This specifically refers to atmospheric correction methods over the ocean by assuming that there is no (or extremely little) water leaving radiance in the near infrared (NIR) and/or short-wave infrared (SWIR) due to the extremely high absorption of light by water in that spectral range. The assumption is typical for atmospheric correction algorithms used with data obtained from many multi-spectral and hyperspectral sensors; see, for example Gao et al. (2000). The large contrast between the water and the land in the NIR and SWIR bands makes it easier to see the effects of many of these artifacts. Because of this, examples of typical coastal areas are presented for many of these artifacts showing the effects to data in the NIR/SWIR bands in scenes with both water and land in the imaged area.

Finally, all of the examples below are either from calibrated data (L_{obs}) or from apparent reflectance [$\rho^*_{obs}=\pi L_{obs}/(\mu_0 E_0)$, where ρ^*_{obs} is the apparent reflectance, L_{obs} is the observed radiance, and $\mu_0 E_0$ is the product of the cosine of the solar zenith angle and the solar irradiance at the top of the atmosphere] data prior to the 2004 flight season. None of the data used in the examples in the following sections has been atmospherically corrected.

[1] Naval Research Laboratory, Code 7232, Washington, DC 20375; Marcos.Montes@NRL.Navy.mil

2. Central blue stripe—scattered light artifact in the center of the swatch

This artifact is present in the AVIRIS ER-2 data. This manifests itself as a faint stripe running down the middle of the image, as shown in Figure 1. It is visibly present in approximately bands 7–28, and is roughly confined to cross-track samples 302–309 (for image cubes with 614 cross-track samples). It is visible in some of the online quick-look imagery, especially over the ocean. Since the ER-2 has a closed cabin, AVIRIS must observe through the ER-2 hatch window. Observation through this window causes the stripe, which is not present in the Twin-Otter data (R. O. Green, 2002; private communication). This feature is present in data since at least 1995, and is in current data. The fractional brightening in these bands is small, and the feature is obvious principally because of its spatial characteristics. The brightening due to the changing geometry of the swells in Fig. 1 is usually much larger, but with much different spectral and spatial characteristics. As the blue stripe appears only in the blue-green bands, it does not cause errors in determining the atmospheric correction parameters. Because atmospheric correction subtracts a large portion of the uniform blue signal across the image, this feature tends to appear with greater contrast after atmospheric correction.

3. Slew

The slew effect is mentioned in the *.readme files that come with the AVIRIS data set. Slew is described as a slight shift in the IFOV when moving from regions of very different brightness. When the detectors move from a bright to a dark area, the next few pixels brighten measurably, as shown in Figs. 2 and 3. The number of pixels affected by slew appears to be a function of the spectrometer, and perhaps band number, as seen in Fig. 3. A typical non-georectified AVIRIS scan line has already been reversed about the center (i.e., swapping pixels 1 and 614, 2 and 613, etc.) before being sent to the user: in the data space, the scanner goes from the right side of the image to the left side[2], but facing forward in the plane, the scanner images from the left to the right. The effect is most noticeable when scanning from bright coasts to darker water, as shown in Fig. 2. Slew, in other words, presents a method of determining the scan direction in some scenes.

The top image in Figure 2 is portion of the data set f010731t01p03_r02, and the bottom is portion of the data set f010731t01p03_r03. These runs were flown in opposite directions [see Table 1 in Montes et al. (2003) for the flight directions], and in these non-georectified images, the right half of f010731t01p03_r02 overlaps with the right half of f010731t01p03_r03 (note, however, that the images in Fig. 2 are sub-images, showing only the rightmost ~350 pixels, i.e., the overlapping area, of each set). The left side of the coasts in each image shows a brightening. The common features in the right side of each image show a brightening that is always to the left of the land, which is geographically the opposite shore in each image. The effects of slew are evident when ratioing (top image in Fig. 3) or differenceing data from adjacent bands that have different slew characteristics, and in cross-track profiles when going from bright to dark areas (bottom plot in Fig. 3).

The effect on atmospheric correction algorithms includes incorrect selections for aerosol model and/or aerosol optical depth for pixels that are a few pixels down scan from the land, which would lead to incorrect water leaving radiances throughout the visible, and therefore incorrect derived products. However, if the pixels affected by slew are not used to derive aerosol parameters, then there is probably little effect on reflectance or products since this effect is again most noticeable in regions of high contrast: going from land that is bright in the NIR/SWIR to water that is dark in the NIR/SWIR. This effect is different from the atmospheric adjacency effect (see, for example, Reinersman and Carder 1995), which also may need to be correctly dealt with in any atmospheric correction scheme. Slew is more limited in spatial scale than the adjacency effect; care should be taken when removing adjacency effect, especially if slew is ignored.

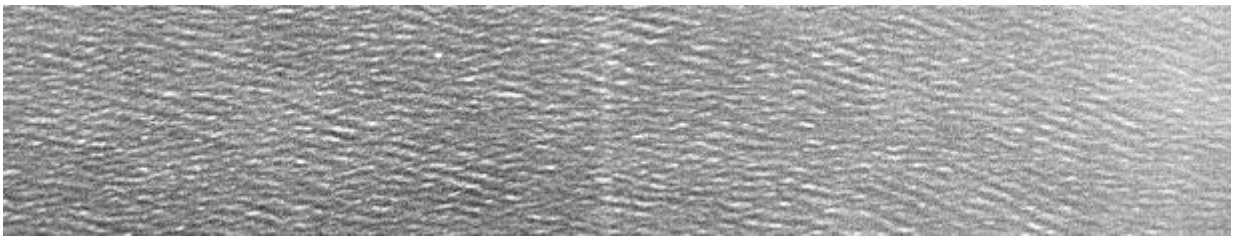

Figure 1. A central blue stripe. This grayscale image is from a section of band 15 of f010731t01p03_r04.

[2] See the "Data Facility" portion of the AVIRIS web page.

Figure 2. Examples of slew. Both the top and the bottom images are the rightmost ~350 samples of non-georectified 1.24 μm band apparent reflectance images processed from AVIRIS collected on 2001 July 31. In these images, a simple land mask (black areas) has been applied for all pixels with NDVI>0.0. The flight direction in each image is from the top of the page to the bottom, and the scan direction is from the right to the left. The flight lines were flown in opposite directions, and portions of the images presented here clearly overlap. One consequence of slew is the brightening of darker pixels in the scan direction when going from a bright (the masked land) to a dark area (the water, here grey). Five landmarks present in each image are labeled A, B, C, D, and E. It is clear that the observed brightening is in the scan direction and *not* an inherent feature of observed land and water.

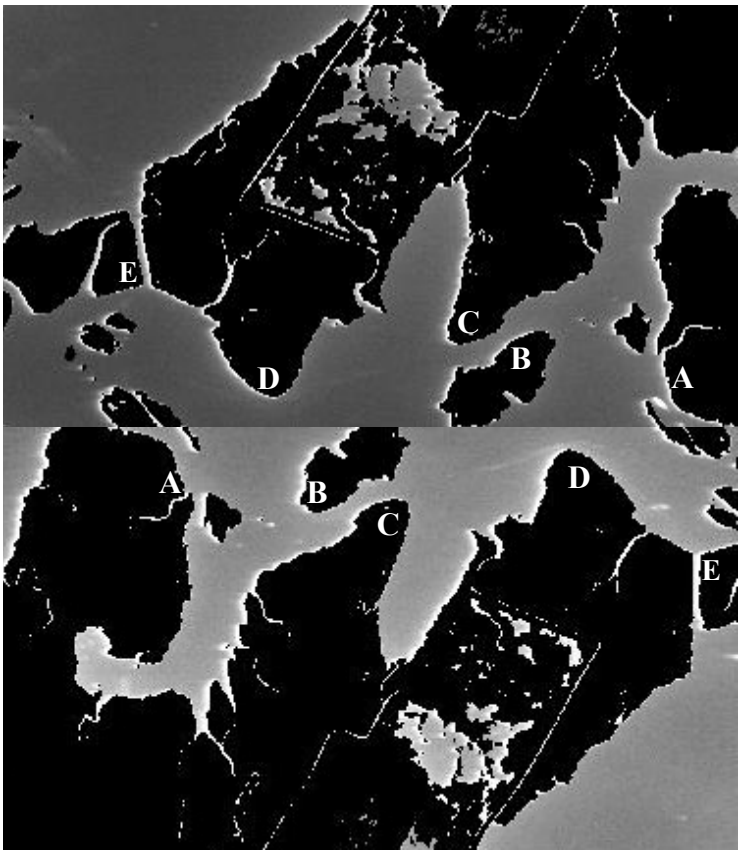

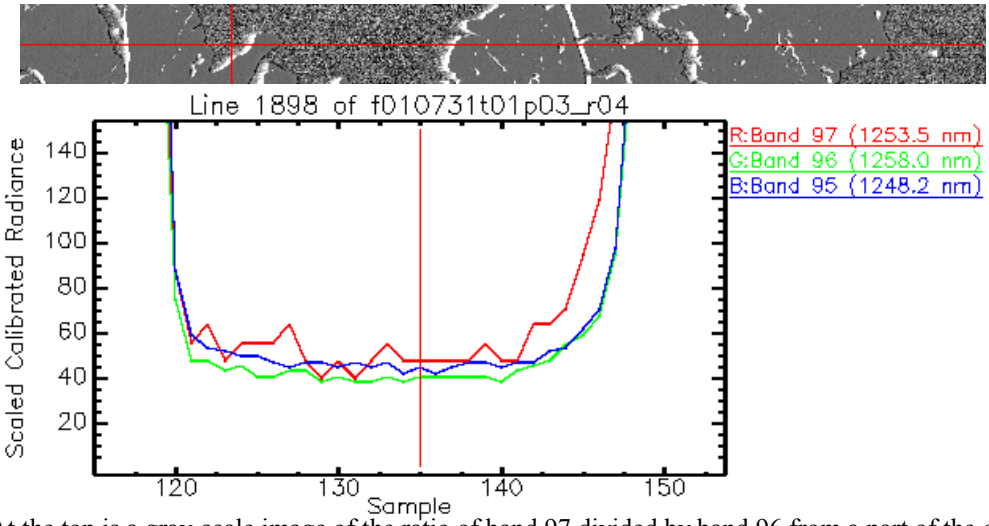

Figure 3. At the top is a gray-scale image of the ratio of band 97 divided by band 96 from a part of the calibrated radiance data from the AVIRIS set f010731t01p03_r04. The ratio increases to > 1.5 (white) going from land (flat grey, μ=1.20, σ=0.07) to water (speckled grey, μ=1.15, σ=0.17). The bottom figure is an x-profile of *radiance* from a portion of the horizontal red line in the upper image. The vertical red line in the lower plot is at the same location as the vertical red line in the upper image. Band 97 takes a longer time to transition from the brighter values on the land to the lower values in the water than either band 95 or 96. All rise at more similar rates when scanning from the darker water to the brighter land. Note that band 97 is on the C spectrometer, while bands 95 and *96 αρε ον τηε Β σπεχτρομετερ, ανδ τηατ* $\lambda_{95} < \lambda_{97} < \lambda_{96}$. The scan direction is from right to left.

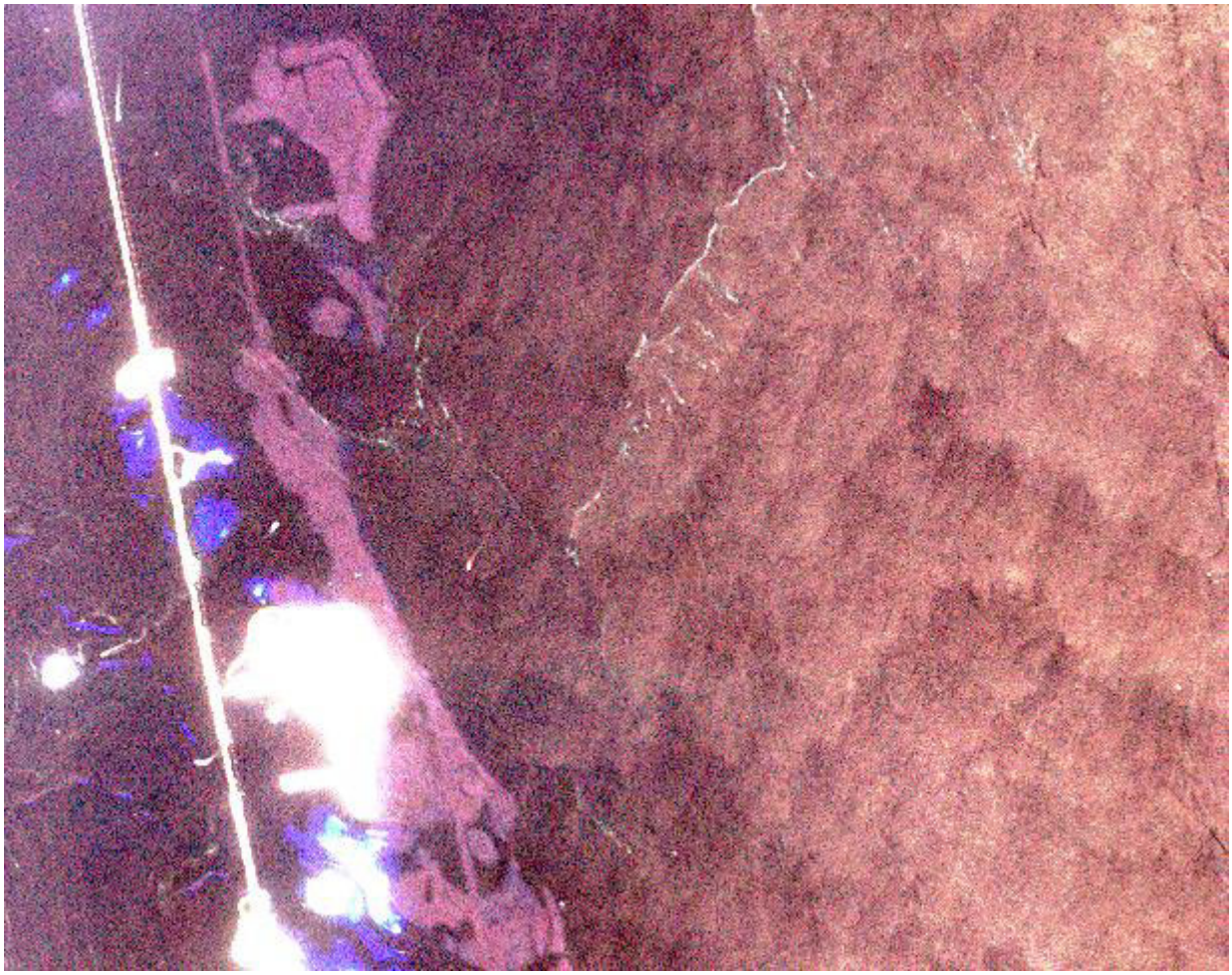

Figure 4. An example of ghosting. This is a portion of f960323t01p02_r10a from the Florida Keys. The flight direction was from the top of this image to the bottom. This 3-color image is from bands 93, 72, and 54, regions of the spectrum where there is strong water absorption. The blue areas are very shallow areas where there is still noticeable signal from the bottom at 867 nm (band 54). The ghosts are obvious, and only appears in 1996 data.

4. Ghost images in 1996 flight year data

The 1996 AVIRIS data has "ghost images" that are most noticeable in areas with both dark backgrounds and bright objects in the field of view, as shown in Fig. 4. This is most easily seen in the NIR/SWIR near water, although it should be present at all wavelengths. In the combination of NIR/SWIR bands used in Fig. 4, the land is saturated and appears white. The ghosts have the same shape and are much dimmer than their source on the land, but clearly of similar magnitude to the signal over the water. The ghosts were due to a window that was used to keep the foreoptics clean. The window, however, introduced some extra reflections and caused the ghosts. This was reported at the 1997 workshop, and was mitigated in 1997, at which time the window was replaced with a door. This door is open only when data is collected. No written record of this ghost exists in the 1998 proceedings (R. O. Green, 2002, private communication). In the NIR, the ghost is usually noticeably brighter than the surrounding water. Using pixels with the ghost images to determine aerosol model and optical depth by assuming the signal is due to only atmosphere and specular reflection causes the wrong aerosol optical depth and/or aerosol model to be selected. Approximately 0.5% of the radiance of the source of the ghost will appear at the location of the ghost. The ghost image appears ~290 pixels (along track) before the actual feature is seen in the data. The number of pixels varies somewhat since ~290 lines are covered in about 24 seconds of time, and the ER-2's orientation may change a fair bit in ~24 seconds. Changes in pitch will affect the displacement in the along-track direction, changes in roll will affect the displacement in the cross-track direction, and changes in heading will affect both; velocity and acceleration variations will also affect the position of the ghost relative to the source. BRDF effects may also play a role in the brightness of the ghost since the source of the ghost is ~13° in front of the image.

5. Band 77

This very noisy band is mentioned in the *.readme files beginning in 2000. This is more problematic over dark images [such as water which absorbs quite strongly at this wavelength (~1.06 μm) and therefore has low signal] than over bright ones. This band needs to be avoided when performing atmospheric correction; unfortunately, this band is in a portion of the spectrum that is relatively free from atmospheric absorption, so it may be used by various atmospheric correction algorithms. Because of this, it is best to delete this band or otherwise to ensure that algorithms do not use this band. Some spectral effects are present in Figs. 1 and 2 of Green et al. (2001). Noise characteristics of this band are easily seen when calculating statistics for a "region of interest" in dark regions of the image.

6. Band 30

Green and Pavri (2001) mentioned the fact that band 30 was excessively noisy in 2000 flight year data. For relatively dark data from an AVIRIS flight in 2001 over a uniform area of Great Bay, New Jersey, the standard deviation in band 30 is about twice that of neighboring bands, and the noise has a visible spatial structure in band 30 images. This band is at about 655 nm, so it is near a rather useful region of the spectrum for ocean studies. It is well worth the time to display this band separately before deciding whether to use data from this band in other data products. The noise is of less consequence for images that are bright in this spectral region.

7. A/B spectrometer overlap region

The A & B spectrometers overlap over a fairly wide spectral range. For the 2001 data, the last three bands of the A spectrometer are very close in wavelength to the first three bands of the B spectrometer. The overlap provides a region to check the cross-calibration between the spectrometers. In order to analyze this effect for a coastal image, scatter plots were generated from the calibrated, non-geocorrected AVIRIS data file f010731t01p03r04_sc04.v1-.img. These scatter plots may be found in Fig. 6. For the oceanic pixels, band 34 is ~ 4.5% brighter than band 31 and band 35 is ~ 7% brighter than band 32. Using the AVIRIS spectral calibration, the wavelength difference is $\lambda_{34} - \lambda_{31} = -0.17$ nm with very similar FWHM; $\lambda_{35} - \lambda_{32} = -2.1$ nm, but $FWHM_{32}/FWHM_{35} = 0.75$. Band 30 is a bit more problematic to analyze because of the obvious spatially structured noise (see §6, above). For ocean and bay pixels, the tendency is for band 30 to be about 6% brighter than band 33, but this is not the case for the brighter land pixels (the bright orange blob in the top plot of Fig. 6). When subtracting ~50% of the signal for atmospheric correction (which is a conservative estimate over water at these wavelengths), the differences become 10% or more. Because of this, it becomes necessary to remove some of the bands in the overlap region so spectra look reasonable. The choice of which bands to keep depends on knowing which bands are better behaved in the sensor, and may also be aided by the availability of field measurements. The characteristics of this overlap region will change, as the AVIRIS instrument is serviced and modified yearly.

8. Adjustment of the spectral calibration

The AVIRIS spectral calibration is determined in the laboratory, under laboratory conditions. As with the radiance calibrations, the best spectral calibration is one that is determined with the sensor in its operating environment. Most spectrometers will require some sort of correction to their laboratory spectral calibration: this effect also occurs in Hyperspectral Digital Imagery Collection Experiment (HYDICE), PHILLS, and HYPERION data. I refer the reader to Gao et al. (2004) and the references therein for a detailed discussion. A summary of the discussion involving AVIRIS is that the correction needed for the spectral calibration changes from year to year: this is not surprising since a lot of work is performed on the AVIRIS instrument between flight seasons. However, the offsets do not appear to change much within a single flight season.

9. Cross-track hatch AR-coating transmittance variation

While attempting to analyze cross-track spectral calibration effects such as smile (e.g., Gao et al. 2002; Gao et al. 2004), we came across a previously unreported AVIRIS artifact. This artifact is probably due to an anti-reflection coating on the ER-2 hatch window (R. O. Green, 2002, private communication). The magnitude appears to be both a function of wavelength as well as cross-track sample number. This effect has been observed in data from 1995, and 2000-2002; it probably exists in all data from the ER-2, but we have not had a chance to examine data from each year. To observe this effect, average a whole non-georectified AVIRIS calibrated radiance cube [224 bands x 614 samples x 512 (or more) lines] down to a single line (224 bands x 614 samples x 1 line). Divide this by the average spectrum of a sample near the central line, avoiding any samples affected by the "blue-stripe" of §2. What is left is the ratio of observed spectra. The solar spectrum and the detector response have been divided out. The remaining quantity is the ratio of the atmospheric and surface reflectance folded together with any cross-track response of the

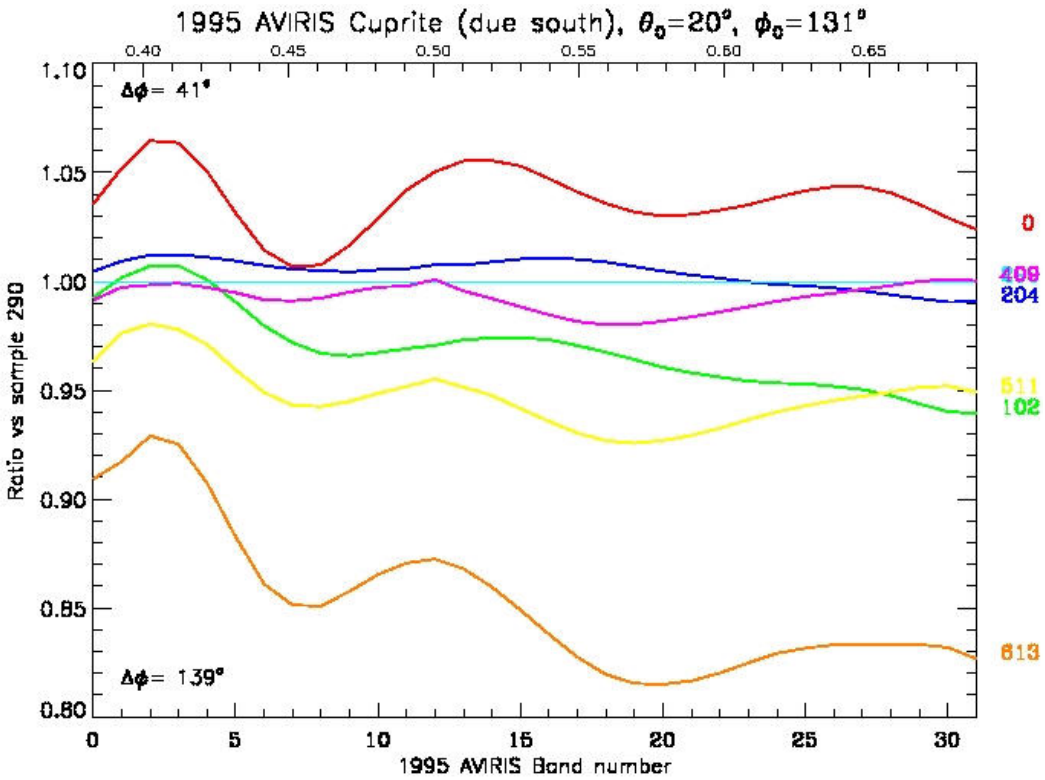

Figure 5, showing an example of the cross-track hatch AR-coating transmittance variation, as derived from a 1995 Cuprite data set. The bottom x-axis is band number, and the top x-axis is the approximate wavelength. The colored curves are associated with the colored labels to the right. The labels are the cross-track sample number, with numbering beginning at 0 as the leftmost pixel in a standard AVIRIS calibrated radiance data set.

complete windows-optics-sensor system. The results, shown in Fig. 5, are a sinusoidal modulation of the first several bands of the A-spectrometer, with a peak-to-peak magnitude of perhaps 5% at the samples furthest from the center. The features are not present in data from the B-spectrometer. These features have been observed over both land and water, in data from many flight seasons.

The effects for atmospheric correction are uncertain, as yet. These bands are not used to determine atmospheric correction parameters over water, and so the effect should be most apparent in products derived from bands in the A spectrometer. This wavelength and sample dependent artifact is a systematic error that can probably be corrected in post-processing. AVIRIS calibration data from a reasonably uniform area (such as the Ivanpah Playa) that spans the field of view will be useful in fully characterizing this effect, as would other methods of removing the variable trends (in which we are not interested) that occur in Fig. 5, leaving only the sinusoidal effect.

10. Algorithmic challenges for low-light imagery

Images of dark areas present challenges other than instrument artifacts. For **any** instrument, atmospheric correction will be difficult if the mean *(μ)* in a particular band in a typical region of interest is less than about 3 times the standard deviation *(σ)*. Spectral regions where this typically occurs are associated with strong atmospheric absorption bands and/or low instrument sensitivity. Over dark water targets in the NIR and SWIR the spectral width of the atmospheric absorption features where $\mu<3\sigma$ increases quite a bit compared with much brighter targets over the land. Spectral regions with this property will not be corrected accurately, and deleting these spectral bands (or some other reasonable treatment) is justified for many low-light imagery scenes.

There are natural features in the data that present continuing challenges for atmospheric correction. Waves and swells are present in much open-ocean data, and are easily resolved at the 20 meter spatial scale of AVIRIS. The atmospheric adjacency effect (i.e., light reflected from the surface from outside the pixel then scattered in the atmosphere into the field of view of the pixel) and the topographic adjacency effect (i.e., the sky does not illuminate

a full 2π steradians of the field of view, and instead some of the light illuminating the pixel in question is directly reflected from trees, mountains, cliffs, buildings, etc.) present features that may be of similar in magnitude to the artifacts presented here. These effects are not due to the sensor. However, in order to correct for these effects in low-light environments, we also need to be able to correct for any instrumental effects in the data that are of similar magnitude.

11. Closing comments

The artifacts presented here are for AVIRIS data prior to the 2004 flight season. It may very well be the case that other artifacts exist, but are not covered here. Those presented here are merely the ones that were noticed in the analysis of AVIRIS data from coastal environments. Some of the artifacts mentioned here have been fixed (the "ghosts of 1996," presented in §4), or are being analyzed and fixed, either in hardware (so as not to affect future data) or in software (and the fixes may then be applicable to archival AVIRIS data). The most serious artifacts in terms of magnitude and pervasiveness in the data are those in §9 (cross-track hatch AR-coating transmittance variation), and, arguably, §3 (slew). Most of the others can be reasonably easily handled by the user by examining and either editing or excising the data (§5, §6, and §7). The spectral calibration (§8) is rectified by adjusting the central wavelength of the spectral bands so that solar and terrestrial absorption features present in the data match those in spectral line databases. As the engineers and scientists associated with the AVIRIS project continue to improve the instrument, one can expect a continuing characterization of the instrument and the mitigation of these and other artifacts.

Acknowledgment

M. Montes received support from the Office of Naval Research.

References

Bindschadler, R., and H. Choi, "Characterizing and Correcting Hyperion Detectors Using Ice-Sheet Images," *IEEE Trans. On Geosci. Rem. Sens.*, 41(6), 1189–1194, 2003.

Conel, J. E., R. O. Green, R. E. Alley, C. J. Bruegge, V. Carrere, J. S. Margolis, G. Vane, T. G. Chrien, P. N. Slater, S. F. Biggar, P. M. Teillet, R. D. Jackson, and M. S. Moran, "In-Flight Radiometric Calibration of the Airborne Visible/Infrared Imaging Spectrometer (AVIRIS)," *SPIE,* Vol. 924, *Recent advances in sensors, radiometry and data processing for remote sensing*, 1988.

Datt, B., T. R. McVicar, T. G. Van Niel, D. L. B. Jupp, and J. S. Pearlman, "Preprocessing EO-1 Hyperion Hyperspectral Data to Support the Application of Agricultural Indices," *IEEE Trans. On Geosci. Rem. Sens.*, 41(6), 1246–1259, 2003.

Gao, B.-C., M. J. Montes, Z. Ahmad, and C. O. Davis, "Atmospheric correction algorithm for hyperspectral remote sensing of ocean color from space," *Applied Optics*, 39(6), 887–896, 2000.

Gao, B.-C., M. J. Montes, and C. O. Davis, "A Curve Fitting Technique to Improve Wavelength Calibrations of Imaging Spectrometer Data," in *Proceedings of the 11th JPL Airborne Earth Science Workshop*, JPL Pub. 03-4, Jet Propulsion Laboratory, Pasadena, California, pp. 99–105, 2002.

Gao, B.-C., M. J. Montes, and C. O. Davis, "Refinement of Wavelength Calibrations of Hyperspectral Imaging Data using a Spectrum-Matching Technique," *Remote Sens. of Env.*, 90(4), pp. 424–433, 2004.

Goetz, A. F. H., B. C. Kindel, M. Ferri, and Z. Qu, "HATCH: Results From Simulated Radiances, AVIRIS and Hyperion," *IEEE Trans. on Geosci. Rem. Sens.*, 41(6), 1215–122, 2003.

Goodenough, D. G., A. Dyk, K. O. Niemann, J. S. Pealman, H. Chen, T. Han, M. Murdoch, and C. West, "Preprocessing Hyperion and ALI for Forest Classification," *IEEE Trans. on Geosci. Rem. Sens.*, 41(6), 1321–1331, 2003.

Green, R. O., J. E. Conel, V. Carrere, C. J. Bruegge, J. S. Margolis, M. Rast, and G. Hoover, "In-flight Validation and Calibration of the Spectral and Radiometric Characteristics of the Airborne Visible/Infrared Imaging Spectrometer (AVIRIS)," *Proc. SPIE Conference on Aerospace Sensing, Imaging Spectroscopy of the Terrestrial Environment*, Orlando, Florida, April 16–20, 1990.

Green, R. O., J. E. Conel, C. J. Bruegge, J. S. Margolis, V. Carrere, G. Vane, and G. Hoover, "In-flight Calibration of the Spectral and Radiometric Characteristics of AVIRIS in 1991," *Summaries of the Third Annual JPL Airborne Geoscience Workshop*, JPL Publication 92-14, Vol. 1, pp. 1–4, Jet Propulsion Laboratory, Pasadena, California, 1992.

Green, R. O., J. E. Conel, M. Helminger, J. van den Bosch, C. Chovit, and T. Chrien, "Inflight Calibration of AVIRIS in 1992 and 1993," *Summaries of the Fourth Annual JPL Airborne Geoscience Workshop*, JPL Publication 93-26, Vol. 1, Jet Propulsion Laboratory, Pasadena, California, October 25, 1993.

Green, R. O., J. E. Conel, M. Helmlinger, J. van den Bosch, and P. Hajek, "In-Flight Radiometric Calibration of AVIRIS in 1994," *Proc. of the Fifth Annual JPL Airborne Earth Science Workshop*, JPL Publication 95-1, Jet Propulsion Laboratory, Pasadena, California, January 23–26, 1995.

Green, R. O., Conel, J. E., Margolis, C. Chovit, and J. Faust, "In-Flight Calibration and Validation of the Airborne Visible/Infrared Imaging Spectrometer (AVIRIS)," *Proc. Sixth Annual Airborne Earth Science Workshop*, JPL Pub. 96-4, Vol. 1, Jet Propulsion Laboratory, Pasadena, California, March 3–5, 1996.

Green R. O., B. Pavri, J. Faust, O. Williams, and C. Chovit, "Inflight Validation of AVIRIS Calibration in 1996 and 1997," *Proc. Seventh Airborne Earth Science Workshop*, JPL Pub. 97-21, Vol. 1, pp. 193–205, Jet Propulsion Laboratory, Pasadena, California, 1998a.

Green, R. O., M. L. Eastwood, and C. M. Sarture, "Imaging Spectroscopy and the Airborne Visible Infrared Imaging Spectrometer (AVIRIS)," *Remote Sens Environ* 65: (3) 227–248 SEP 1998b.

Green, R. O., B. Pavri, J. Faust, C. Chovit, and O. Williams, "AVIRIS In-Fight Radiometric Calibration Results for 1998," *Proc. Eighth Airborne Earth Science Workshop*, JPL Publication 99-17, Vol. 1, pp. 161–175, Jet Propulsion Laboratory, Pasadena, California, 1999.

Green, R. O., and B. Pavri, "AVIRIS Inflight Calibration Experiment, Measurements, Analyses and Results, Sensitivity Analysis and Intraflight Stablity," *Proc. Ninth Airborne Earth Science Workshop*, JPL Publication 00-18, pp. 207–222, Jet Propulsion Laboratory, Pasadena, California, 2000.

Green, R. O., T. Chrien, and C. Sarture, "Exploring a Black Body Source as an Absolute Radiometric Calibratoin Standard and Comparison with a NIST Traced Lamp Standard," in *Proceedings of the Tenth JPL Airborne Earth Science Workshop*, JPL Pub. 02-1, Jet Propulsion Laboratory, Pasadena, California, pp. 193–203, 2001.

Green, R. O., and B. Pavri, "AVIRIS Inflight Calibration Experiment Measurements, Analyses, and Results in 2000," in *Proceedings of the Tenth JPL Airborne Earth Science Workshop*, JPL Pub. 02-1, Jet Propulsion Laboratory, Pasadena, California, pp. 205–218, 2001.

Green, R. O., and B. Pavri, "AVIRIS Inflight Calibration Experiment Results for 2001," in *Proceedings of the 11th JPL Airborne Earth Science Workshop*, JPL Pub. 03-4, Jet Propulsion Laboratory, Pasadena, California, pp. 125–137, 2002.

Green, R. O., and B. Pavri, "Inflight Calibration Experiment Results for AVIRIS on May 6, 2002 at Rogers Dry Lake, California," *Proceedings of the 12th Airborne Earth Science Workshop,* JPL Pub. 04-6, Jet Propulsion Laboratory, Pasadena, California, pp. 109–120, 2003.

Green, R. O., B. E. Pavri, and T. G. Chrien, "On-Orbit Radiometric and Spectral Calibration Characteristics of EO-1 Hyperion Derived with an Underflight of AVIRIS and *In Situ* Measurements at Salar de Arizaro, Argentina," *IEEE Trans. On Geosci. Rem. Sens.*, 41(6), 1194–1203, 2003.

Leathers, R. A., T. V. Downes, W. A. Snyder, J. H. Bowles, C. O. Davis, M. E. Kappus, W. Chen, D. Korwan, M. J. Montes, W. J. Rhea, and M. E. Carney, "Ocean PHILLS Data Collection and Processing: May 2000 Deployment, Lee Stocking Island, Bahamas," NRL/FR/7212—02-10,010, 2002.

Montes, M. J., B.-C. Gao, C. O. Davis, and M. Moline, "Analysis of AVIRIS Data from Leo-15 Using Tafkaa Atmospheric Correction," *Proceedings of the 12th Airborne Earth Science Workshop,* JPL Pub. 04-6, Jet Propulsion Laboratory, Pasadena, California, pp. 212–218, 2003.

Pearlman, J. S., P. S. Barry, C. C. Segal, J. Shepanski, D. Beiso, and S. L. Carman, "Hyperion, a Space-Based Imaging Spectrometer," *IEEE Trans. on Geosci. Rem. Sens.*, 41(6), 1160–1173, 2003.

Reinersman, P. N., and K. L. Carder, "Monte Carlo simulation of the atmospheric point-spread function with an application to correction for the adjacency effect," *Appl. Opt.*, 34, 4453–4471, 1995.

Snyder, W. A., C. O. Davis, J. H. Bowles, B.-C. Gao, D. Gillis, D. Korwan, G. Lamela, M. Montes, and W. J. Rhea, "PHILLS-1 Hyperspectral Data Processing: 2001 LEO-15 Deployment," NRL/FR/7230—04-10,060, 2004.

(TGARS) *Special Issue on the Earth Observing (EO-1) Mission, IEEE Trans. on Geosci. Rem. Sens.,* 41(6), pp. 1147–1414, June 2003.

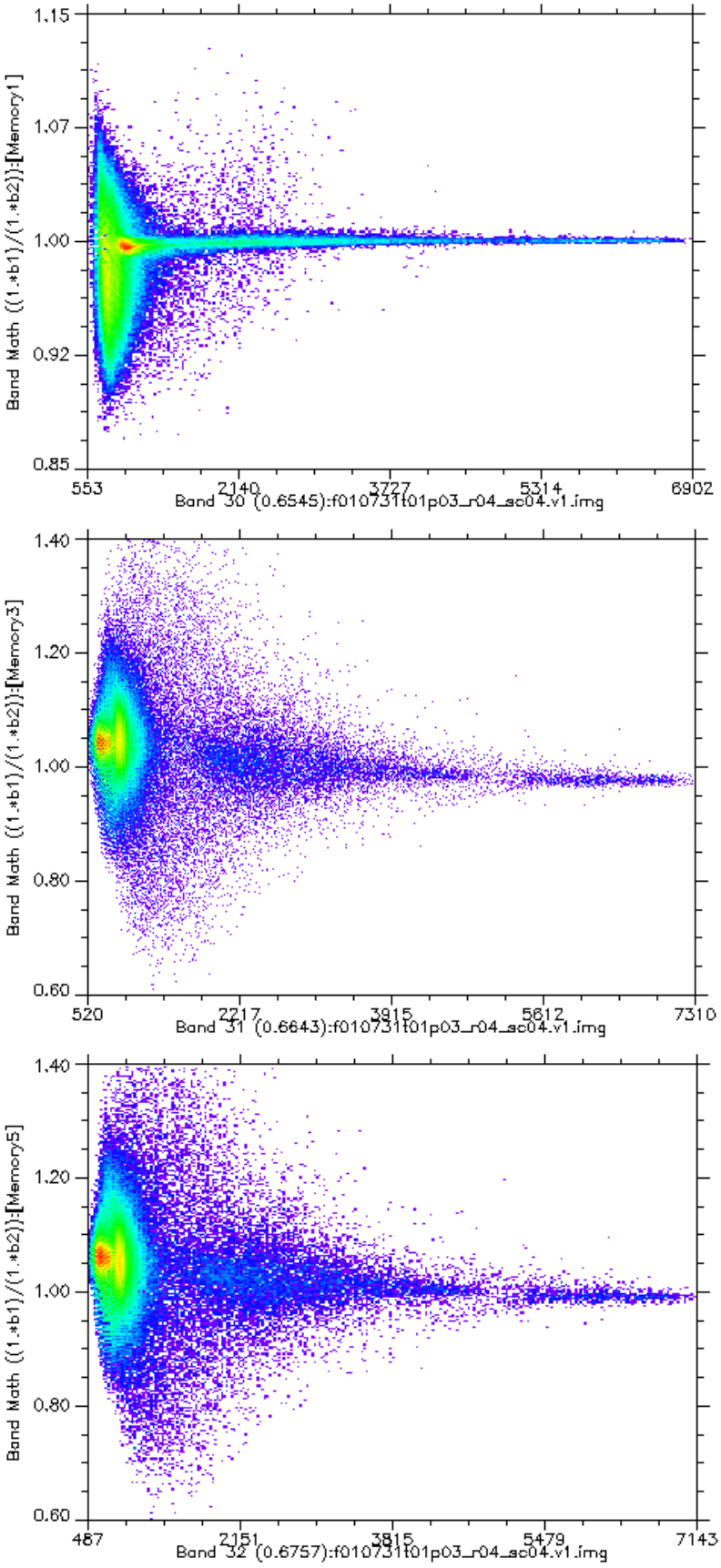

Figure 6. Scatter plots of near-overlapping bands from the A/B spectrometer region. Please note that the abcissa and ordinate have different scales on each of the three plots. The quantities plotted are: the ratio of band 33 to band 30 vs. band 30 (*top*); the ratio of band 34 to band 31 vs. band 31 (*middle*); and the ratio of band 35 to band 32 vs. band 32 (*bottom*). Colors indicate the density of points in each region, with red being the highest density and purple being the lowest density.

Pixels from the ocean and bay are in the leftmost yellow strip in the top, and in the bright red/orange blobs on the left in the middle and bottom scatter plots. In fact, the red/orange indicates that a very large majority of the pixels are in those neighborhoods.

Pixels from land areas make up the orange blob (top) and the yellow blobs (bottom and middle) somewhat to the right (i.e., higher values of the abcissa) of the pixels from the ocean or bay.